Microscopy of extreme ultraviolet lithography masks with 13.2 nm tabletop laser illumination

F. Brizuela,* Y. Wang, C. A. Brewer, F. Pedaci, W. Chao, E. H. Anderson, Y. Liu, K. A. Goldberg, P. Naulleau, P. Wachulak, M. C. Marconi, D. T. Attwood, J. J. Rocca, and C. S. Menoni

National Science Foundation Engineering Research Center for Extreme Ultraviolet Science and Technology, Colorado State University, Fort Collins, Colorado 80523, USA

Center for X-ray Optics, Lawrence Berkeley National Laboratory, Berkeley, California 94720, USA

**Corresponding author: brizuela@engr.colostate.edu*

Received October 7, 2008; accepted November 12, 2008;
posted December 16, 2008 (Doc. ID 102373); published January 26, 2009

We report the demonstration of a reflection microscope that operates at 13.2 nm wavelength with a spatial resolution of 55±3 nm. The microscope uses illumination from a tabletop extreme ultraviolet laser to acquire aerial images of photolithography masks with a 20 s exposure time. The modulation transfer function of the optical system was characterized. © 2009 Optical Society of America

OCIS codes: 110.7440, 140.7240, 180.7460.

Extreme ultraviolet lithography (EUVL) is the leading technology for integrated circuit fabrication at the 22 nm half-pitch node, and a contender technology for the 32 nm node. The successful implementation of this approach relies on the availability of EUVL masks free of printable defects. Therefore, there are pressing demands for the development of metrology tools capable of finding and characterizing printable amplitude and phase defects on the masks. The masks' resonant-reflective multilayer coatings and wavelength-specific response dictate the necessity of extreme ultraviolet (EUV)-wavelength inspection.

Several techniques can be employed to detect and characterize mask defects. Scanning methods, based on deep ultraviolet light are highly efficient for detecting defects but are incapable of assessing their EUV-wavelength-specific morphology [1–3]. Instead, for defect characterization, full-field microscopes that operate at wavelengths around 13.5 nm, within the bandwidth of Mo/Si multilayer coatings, and that can render high-resolution aerial images of the mask surface can be used. These actinic tools, when designed to mimic the imaging characteristics of production EUVL steppers, produce a magnified aerial image of the mask that allows the evaluation of pattern and defect printability, independent of the response of the photoresist. Furthermore, these microscopes can be useful in defect repair evaluation of EUVL masks [2]. Demonstrations of actinic aerial microscopes have until now been conducted at synchrotron facilities where radiation from bending magnets provides the required illumination [4,5]. These microscopes are capable of imaging amplitude and phase defects with a spatial resolution better than 100 nm [6].

Transitioning EUV full-field microscopes into compact devices for on-site EUVL mask inspection with short exposure times requires compact light sources that provide sufficient flux near 13.5 nm wavelength. Low-resolution imaging systems capable of locating defects but not of resolving their morphology have been demonstrated using compact EUV incoherent sources [7]. Owing to their high brightness, tabletop EUV lasers are attractive illumination sources for compact high-resolution microscopy [8,9]. A 13.2 nm wavelength tabletop microscope capable of rendering images of transmissive samples with a spatial resolution better than 38 nm has been demonstrated [10]. However, to our knowledge the more challenging reflection-mode microscopy at this wavelength has not yet been realized. In this Letter we report what we believe is the first demonstration of an actinic tabletop EUV reflection microscope that captures images in 20 s with a half-pitch spatial resolution of approximately 55 nm, comparable to that obtained with synchrotron sources.

The microscope uses as its illumination source a tabletop, plasma-based, collisional EUV laser that operates at a wavelength of 13.2 nm [11,12]. This source is well suited for actinic mask inspection, because Mo/Si multilayers have a reflectivity of about 55% at this wavelength. Furthermore, this wavelength that falls on the rising edge of the multilayer's reflectivity curve might be more sensitive to detect subtle phase errors in the EUVL masks. The laser beam is created by the amplification of spontaneous emission in a transient population inversion produced by electron impact excitation in a transition of nickel-like Cd ions. To generate the EUV laser pulses a plasma is created by heating a Cd slab target with a sequence of pulses from a chirped-pulse-amplification Ti:sapphire laser system. Prepulses are focused into a 30-μm-wide$\times$4-mm-long line, to generate a Cd plasma that is allowed to expand to reduce electron density gradients [11,12]. A transient population inversion is subsequently achieved by rapidly heating the plasma with an intense ($\sim 1\times 10^{14}$ W cm^{-2}) 6.7 ps duration pulse impinging at a grazing incidence angle of 23°. The laser is operated at 5 Hz repetition rate, producing a highly monochromatic ($\Delta\lambda/\lambda < 1\times 10^{-4}$) beam with a moderate spatial coherence (1/20 of the beam diameter) and an average power of ~ 1 μW [13].

The reflection microscope, housed in a 70 cm $\times$ 45 cm $\times$ 40 cm vacuum chamber, is illustrated schematically in Fig. 1(a). The laser beam is directed by a

0146-9592/09/030271-3/$15.00

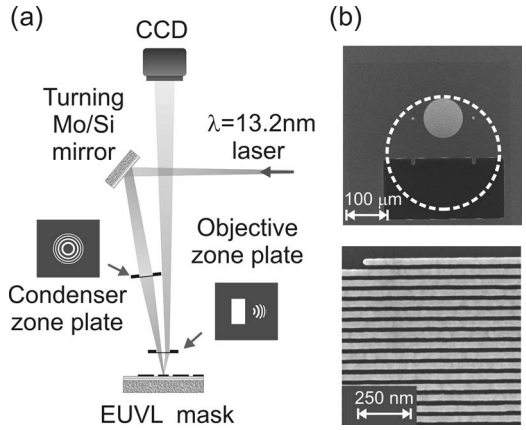

Fig. 1. (a) Schematic illustration of the microscope (not to scale). (b) Scanning electron microscopy (SEM) images of (top) the off-axis zone plate and uncoated window region, where the dashed line indicates the extent of the "parent" zone plate, and (bottom) 40 nm half-pitch outer zones of the objective zone plate.

42° incidence Mo/Si-coated flat mirror onto a condenser zone plate that focuses the light onto the sample. The reflected light is projected by an off-axis zone plate objective, forming an image on an EUV-sensitive back-illuminated CCD detector.

The condenser and objective zone plates were fabricated by electron beam lithography on a 40-nm-thick Ni layer deposited onto 100-nm-thick Si_3N_4 membranes [14]. The 5-mm-diameter condenser zone plate has an outer zone width of 100 nm, which sets its focal length and numerical aperture (NA_c) to 38 mm and 0.066, respectively, at 13.2 nm wavelength. Its efficiency is ~5%. The condenser is slightly overfilled by the laser light and illuminates the EUV mask at a 6° angle of incidence from normal. This geometry mimics the mask illumination conditions of a 4× demagnification EUVL stepper with a NA of 0.25 [15]. Figure 1(b) shows a SEM image of the objective zone plate. The objective zone plate is an off-axis subaperture of a full parent zone plate lens that would have a 330 μm diameter (dashed line in the figure), an outer zone width of 40 nm, and a focal length of 1 mm. The pupil diameter is 120 μm, defining a NA of 0.0625, and its center is displaced 100 μm from the axis of the parent zone plate. An uncoated rectangular aperture next to the off-axis objective zone plate transmits the incoming condensed laser beam illumination. To increase the transmission through this aperture, the Si_3N_4 membrane was thinned to 40 nm. The off-axis zone plate enables near-normal incidence imaging of the mask surface, minimizes aberrations, and provides incoherent illumination conditions by matching the NA of the condenser [16].

The imaged object in these experiments was the surface of a Mo/Si multilayer mirror patterned with Ni absorber grating structures with half-pitch sizes ranging from 80 to 500 nm. EUV images of four elbow patterns with 80, 100, 120 and 140 nm half-pitch are shown in Fig. 2 along with their respective intensity cross sections (lineouts). The images were obtained using a 20 s exposure time, with the laser operating at a repetition rate of 5 Hz. The images have a field of view of approximately 5 μm × 5 μm. They were taken with a magnification of 610× at which each pixel on the CCD corresponds to 22 nm in the sample plane. The images show no distinguishable coherence effects as expected for a practically incoherent optical system.

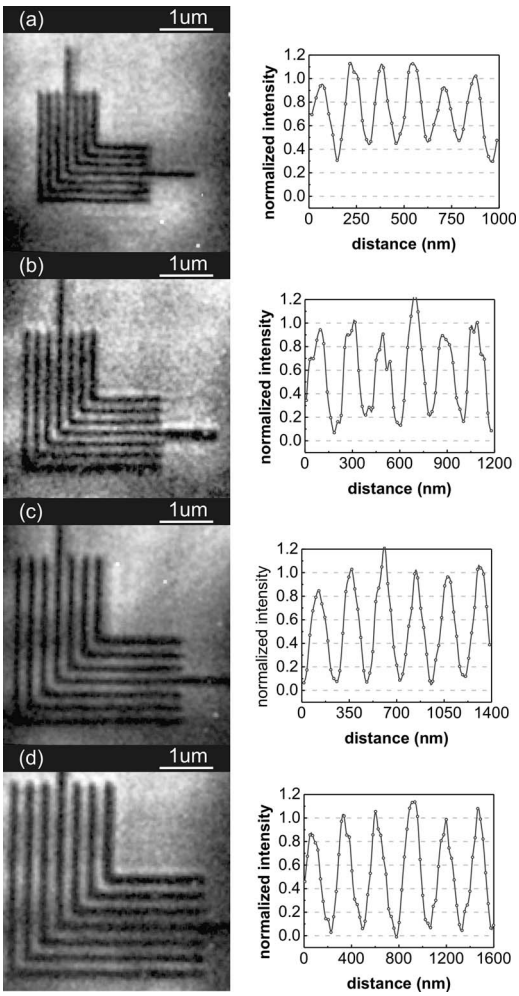

Fig. 2. Fully resolved actinic images and intensity lineouts of elbow patterns with (a) 80, (b) 100, (c) 120, and (d) 140 nm half-pitch. The images were obtained with 20 s exposures and ~610× magnification. The intensity lineouts were obtained by averaging five rows of pixels (~100 nm on the mask) across the gratings.

The modulation transfer function (MTF) of the microscope, shown in Fig. 3, was constructed using the intensity modulation data from Fig. 2. The modulation $[M=(I_{max}-I_{min})/I_{max}]$ starts to roll off for structures smaller than 120 nm half-pitch, in agreement with simulations for a 0.0625 NA objective under incoherent illumination. At 80 nm half-pitch the measured intensity modulation is approximately 65%, a value significantly higher than the Rayleigh resolution value of 26.5%. This indicates that the spatial resolution of the microscope is below 80 nm.

In the absence of gratings structures with lines smaller than 80 nm, the characterization of the instrument's MTF was extended using a knife-edge test (Fig. 4). For incoherent imaging conditions the 10%

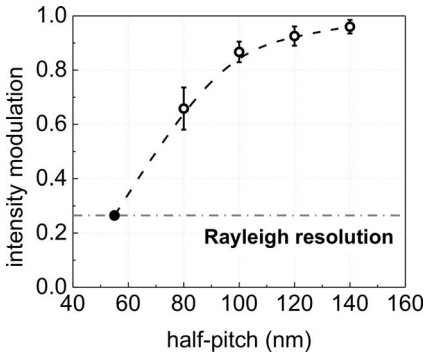

Fig. 3. Microscope's MTF constructed using the lineouts from the images of Fig. 2 (open circles) and the knife-edge test (solid circle).

to 90% intensity transition across a sharp edge corresponds to twice the half-pitch grating resolution of the optical system [16]. The measurements yielded a 10% to 90% transition of 110±5 nm, corresponding to a half-pitch grating spatial resolution of 55±3 nm.

The spatial resolution of the microscope was independently confirmed by analyzing the EUV images of Fig. 2 with a full-image correlation method described by Wachulak *et al.* [17]. Using this correlation method, a half-pitch resolution of 53±10 nm was obtained. This resolution meets the specifications set for the EUVL 22 nm technology half-pitch node.

In summary, we have demonstrated an actinic tabletop EUV reflection microscope that, emulating the incoherent illumination conditions of a EUVL stepper, can obtain images of absorber patterns in Mo/Si EUVL masks with a spatial resolution of 55 nm in 20 s exposures. It is forecasted that improvements in the throughput of the imaging system will reduce exposure times to a few seconds.

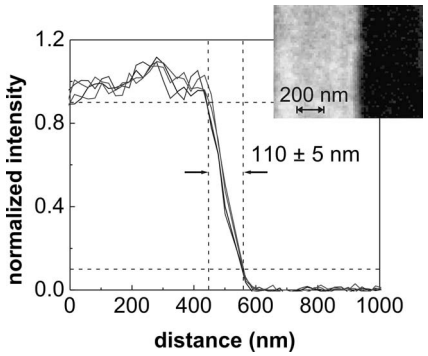

Fig. 4. Knife-edge test for the EUV image shown in the insert. The 10% to 90% transition is 110±5 nm.

We acknowledge the contribution of Georgiy Vaschenko and the support of the Engineering Research Centers Program of the National Science Foundation (NSF) under NSF Award EEC-0310717.

References

1. K. A. Goldberg, A. Barty, Y. Liu, P. A. Kearney, Y. Tezuka, T. Terasawa, J. S. Taylor, H.-S. Han, and O. R. I. Wood, J. Vac. Sci. Technol. B **24**, 2824 (2006).
2. K. A. Goldberg, A. Barty, P. Seidel, K. Edinger, R. Fettig, P. A. Kearney, H.-S. Han, and O. R. I. Wood, Proc. SPIE, **6517** 6511 (2007).
3. K. A. Goldberg, S. B. Rekawa, C. D. Kemp, A. Barty, E. H. Anderson, P. A. Kearney, and H.-S. Han, Proc. SPIE **6921**, 6143 (2008).
4. K. A. Goldberg, Proc. SPIE **6730**, 67305E-1-12 (2007).
5. H. Kinoshita, K. Hamamoto, N. Sakaya, M. Hosoya, and T. Watanabe, Jpn. J. Appl. Phys. Part 1 **46**, 6113 (2007).
6. K. A. Goldberg, P. Naulleau, I. Mochi, E. H. Anderson, S. B. Rekawa, C. D. Kemp, R. F. Gunion, H.-S. Han, and S. Huh, J. Vac. Sci. Technol. B **26**, 2220 (2008).
7. Y. Tezuka, T. Tanaka, T. Terasawa, and T. Tomie, Jpn. J. Appl. Phys. Part 1 **45**, 5359 (2006).
8. F. Brizuela, G. Vaschenko, C. Brewer, M. Grisham, C. S. Menoni, M. C. Marconi, J. J. Rocca, W. Chao, J. A. Liddle, E. H. Anderson, D. T. Attwood, A. V. Vinogradov, I. A. Artioukov, Y. P. Pershyn, and V. V. Kondratenko, Opt. Express **13**, 3983 (2005).
9. C. A. Brewer, F. Brizuela, P. Wachulak, D. H. Martz, W. Chao, E. H. Anderson, D. T. Attwood, A. V. Vinogradov, I. A. Artyukov, A. G. Ponomareko, V. V. Kondratenko, M. C. Marconi, J. J. Rocca, and C. S. Menoni, Opt. Lett. **33**, 518 (2008).
10. G. Vaschenko, C. Brewer, E. Brizuela, Y. Wang, M. A. Larotonda, B. M. Luther, M. C. Marconi, J. J. Rocca, and C. S. Menoni, Opt. Lett. **31**, 1214 (2006).
11. J. J. Rocca, Y. Wang, M. A. Larotonda, B. M. Luther, M. Berrill, and D. Alessi, Opt. Lett. **30**, 2581 (2005).
12. Y. Wang, M. A. Larotonda, B. M. Luther, D. Alessi, M. Berrill, V. N. Shyaptsev, and J. J. Rocca, Phys. Rev. A **72**, 053807 (2005).
13. Y. Liu, Y. Wang, M. A. Larotonda, B. M. Luther, J. J. Rocca, and D. T. Attwood, Opt. Express **14**, 12872 (2006).
14. E. H. Anderson, IEEE J. Quantum Electron. **42**, 27 (2006).
15. A. Barty, J. S. Taylor, R. Hudyma, E. Spiller, D. W. Sweeney, G. Shelden, and J.-P. Urbach, Proc. SPIE **4889**, 1073 (2002).
16. J. M. Heck, D. T. Attwood, W. Meyer-Ilse, and E. Anderson, J. X-Ray Sci. Technol. **8**, 95 (1998).
17. P. W. Wachulak, C. A. Brewer, F. Brizuela, C. S. Menoni, W. Chao, E. H. Anderson, R. A. Bartels, J. J. Rocca, and M. C. Marconi, J. Opt. Soc. Am. B **25**, B20 (2008).